ACS APPLIED POLYMER MATERIALS

pubs.acs.org/acsapm Article

Polydimethylsiloxane-Based Mechanoluminescent Occlusal Splint with the Visualization of Occlusal Force

Yue Han, Yongqing Bai, Jiali Bian, Xiuping Guo, Bin Liu,* and Zhaofeng Wang*

Cite This: *ACS Appl. Polym. Mater.* 2021, 3, 5180−5187 Read Online

ACCESS | Metrics & More | Article Recommendations

ABSTRACT: The occlusal splint is a common medical device that is used to treat temporomandibular disorders. However, the current commercial occlusal splints still have several disadvantages in terms of flexibility, abrasion resistance, and occlusal inspection. In this work, ZnS:Mn^{2+}/polydimethylsiloxane composite elastomers were prepared, and the mechanical and biological properties were investigated to evaluate their potential as occlusal splint materials. The results suggest that compared to the commercial occlusal splint material, ZnS:Mn^{2+}/polydimethylsiloxane exhibits desirable flexibility, improved wear resistance, and excellent biocompatibility and antibacterial properties. In addition, the elastomer shows intense and stable mechanoluminescence under oral conditions with a linear relationship to the applied load. This further provides a visualized approach for the convenient and real-time detection of occlusal high points. Based on the above results, a mechanoluminescent occlusal splint model was fabricated, which is promising to be applied in occlusal splint therapy applications.

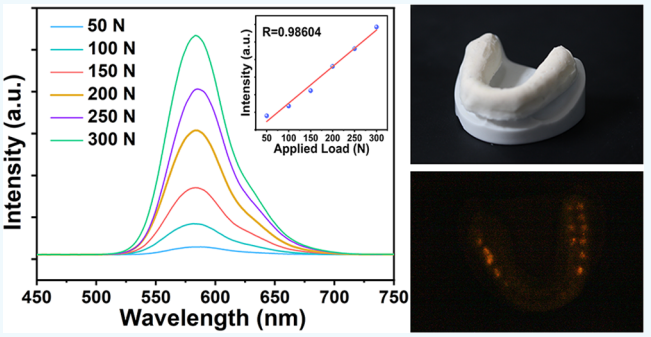

KEYWORDS: *soft occlusal splint, biological performance, mechanoluminescence, mechanics visualization, occlusal detection*

1. INTRODUCTION

Temporomandibular disorders (TMD) are a heterogeneous group of oral clinical diseases, affecting widely oral and maxillofacial structures with the chief symptom of pain/discomfort.[1−4] The incidence of TMD in the population is about 3.7−12%, which is up to 3−5 times in women,[5] especially. In recent reports, there are significant statistical differences in occlusal parameters of TMD patients, comparing to the normal, including imbalance and asymmetry between occlusal force and occlusal center distance.[6] The occlusion characteristics of TMD patients are highly correlated with the degree and type of diseases.[7] As a conservative treatment device for TMD, occlusal splints are widely used because of their effectiveness, reversibility, and non-damage.[2,8−11] Among them, the soft occlusal splint has the advantages of outstanding elasticity and marvelous adaptability,[12] showing excellent effectiveness in the treatment of temporomandibular joint disease.[13,14] By relaxing the muscle and reassigning occlusal force, the occlusal splint establishes a new biomechanical equilibrium between occlusion and muscle to achieve the purpose of treatment.[15] This process often requires long-term use of the device accompanied by multiple periodic reexaminations. During the treatment procedure, dentists need to detect the occlusal force to find the occlusal fulcrum on the surface of the occlusal plate and adjust the occlusal splint to achieve a uniform and balanced occlusion.[14,16]

At present, commercial splint materials, including ethylene-vinylacetate (EVA), polymethylmethacrylate (PMMA), polycarbonate (PC), polyethere-therketone (PEEK), and polyethylene-terephthalate (PETG), have significant deficiency of wear resistance performance to a certain extent during long-term usage,[17−19] which are always difficult to modify due to the soft material properties. In addition, it has been reported that the existing commercial occlusal splint materials have high water absorption and solubility and strength attenuation at oral temperature, which cannot meet the current ANSI and SAI standards.[20] In addition to the insufficient performance, there are still some difficulties for occlusal splints to achieve equilibrium occlusion. As a necessary treatment procedure in TMD treatment,[21] occlusal analysis has developed many different occlusal indicators in the oral discipline, including the most widely used paper, T-Scan sensor, silk, and so on.[22] It has been reported that the current occlusal detection products cannot accurately reflect the actual occlusion after testing.[23] The occlusal indicator changes the surface electromyography

Received: July 25, 2021
Accepted: August 23, 2021
Published: September 1, 2021

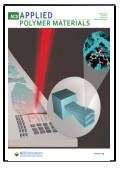

(SEMG) activity during occlusion, which may affect the effectiveness of occlusal analysis.[24] Besides the effects of their thickness and saliva infiltration, the reliability of mark size and applied occlusal load is not linearly correlated. Thus, the occlusion imprints of articulating paper cannot provide clinicians with reliable references regarding the magnitude of occlusal forces.[25−27] Therefore, it is necessary to find an alternative material that can provide accurate occlusal inspection function and better abrasion resistance and solubility resistance.

Mechanoluminescence (ML), a luminescent phenomenon stimulated by mechanical force,[28,29] has been widely used in stress sensing,[29] heartbeat detection,[30] encryption, anticounterfeiting,[31] and other fields, with the advantage of being energy saving and environmental protection.[32] It is found that most of the ML materials are inorganic powders with excellent physical and chemical stability, which could be introduced in a certain matrix to produce various ML composites.[33] Particularly, ML powders could be composited with flexible matrices to generate ML elastomers. Because ML directly establishes the relationship between mechanics and luminescent signals, the fabrication of ML elastomers provides us a strategy to realize the occlusal analysis in a way of mechanics visualization.[34] As an alternative occlusion material, the ML elastomer should also have good mechanics and biological performance, which suggests that the employed flexible matrix for the ML elastomer is of great importance. Polydimethylsiloxane (PDMS) is frequently used as the matrix for ML powders because of its high optical transparency, efficient stress transfer ability, and easy fabrication.[35,36] Moreover, PDMS shows excellent biocompatibility and permeability, high-temperature resistance, and natural hydrophobicity.[37−39] Therefore, the elastomer composed of ML powders and PDMS matrices is promising to replace the existing occlusal materials to possess better overall performance and visualized occlusal inspection.

Herein, in this work, we employed the typical ZnS:Mn^{2+} ML powders (one of the most efficient ML materials) and the flexible PDMS matrix as the components to fabricate the ML elastomer and evaluate its potential as an occlusal splint material. The results suggest that compared to the commercial occlusal material, the as-fabricated ML elastomer shows better performance on flexibility, wear resistance, biocompatibility, antibacterial activity, and stability. Particularly, the emitted ML signals show a linear relationship to the applied load, providing a facile and visualized way on the occlusal force to establish the occlusal balance.

2. EXPERIMENTAL DETAILS

2.1. Synthesis of ZnS:Mn^{2+} Powders. ZnS:Mn^{2+} was synthesized by a high-temperature solid-state reaction, employing ZnS (99.99%) and $MnCO_3$ (99.95%) as the raw materials. According to previous reports, the doping concentration of Mn^{2+} was set to be 1%.[33,40,41] First, 10.5112 g of ZnS and 0.1239 g of $MnCO_3$ were weighed and mixed in an agate mortar. Then, the mixture was transferred in an alumina crucible and sintered at 1150 °C for 3 h in a tube furnace (GSL-1600X) in an inert atmosphere (100% N_2). After cooling to room temperature, ZnS:Mn^{2+} phosphors were obtained and stirred thoroughly for further use.

2.2. Fabrication of ZnS:Mn^{2+}/PDMS Composite Elastomers for Performance Analysis. To quantitatively analyze the ML properties, ZnS:Mn^{2+} powder was mixed in the PDMS precursor inside of a silicon rubber mold with weight ratios of 1:10, 2:10, 3:10, 4:10, and 5:10. After completely mixing, the uncured mixture was degassed in a vacuum oven (room temperature; vacuum degree: −80 KPa) for 2 min to remove bubbles. Eventually, the mixture was cured in an oven at 80 °C for 1 h, and the ZnS:Mn^{2+}/PDMS elastomers were obtained.

2.3. Fabrication of ZnS:Mn^{2+}/PDMS Occlusal Splint. In order to fabricate the ZnS:Mn^{2+}/PDMS occlusal splint, an alginate mold was first taken from the patient's mouth to further produce the gypsum model of a single jaw. After high-temperature heating, wax was used to make the shape of the occlusal plate on the surface of the gypsum model, and then another gypsum model was made on the other side of the wax. By removing the middle wax, the mixture of ZnS:Mn^{2+} and PDMS was filled between the upper and the lower gypsum molds, and a splint was obtained after curing at 80 °C for 1 h.

2.4. MTT Assay. L929 mouse fibroblasts (ATCC, Rockville, MD, USA) were used for biocompatibility assessment of the ZnS:Mn^{2+}/PDMS elastomers. Each elastomer sample was prepared with a size of 10 × 10 × 1 mm and sterilized under ultraviolet (UV) overnight. The culture medium for cell proliferation was a mixture based on Dulbecco's modified Eagle's medium (DMEM, Gibco, USA) combined with penicillin−streptomycin (100 IU/mL), D-glucose (4.5 g/L), and fetal bovine serum (10%, Australia Origin, Gibco, USA). Also, the proliferation conditions of L929 cells were set at 37 °C and 5% aseptic CO_2. Then, the ZnS:Mn^{2+}/PDMS elastomers with different ratios of ZnS:Mn^{2+} powder were put into a 24-well plate with 104 L929 cells in each well. At different times (1, 3, 5, and 7 days), 100 μL of MTT solution (St. Louis, MO, USA) was dropped into each well. Then, 750 μL of dimethyl sulfoxide (DSMO) were added to each well to dissolve the blue formazan reaction product after another 4 h. Then, a microplate reader (Bio-Rad iMark) was used to measure the average absorbance value after 150 mL of dissolve solution was transferred to a 96-well plate, which was repeated 3 times. A control group with only L929 cell suspension was set for comparison. Eventually, the biocompatibility was analyzed and obtained by comparing the absorbance values between the experimental and control groups.

2.5. Antibacterial Assessment. The ZnS:Mn^{2+}/PDMS elastomer with different concentrations of ZnS:Mn^{2+} powder and PETG elastomer (the control group) were prepared as 10 × 10 × 1 mm and irradiated under UV light. After resuscitating *Streptococcus mutans* (*S. mutans*, UA159), the mutans were cultured at 37 °C for 24 h. Then, the single colony was placed in a BHI medium and cultured overnight in a shaker at 150 rpm. Eventually, the bacterial concentration was adjusted to 10^8 CFU/mL. And then, the bacterial suspension was diluted 1000 times to 10^5 CFU/mL. Then, 1 mL of bacterial solution was dropped on the surface of the elastomer samples in the Petri dish, and the surface was adhered to the sterilized polyethylene film. After 24 h of culture, 20 mL of PBS was used to rinse the surface, and the rinse solution was transferred to a conical flask, shaken well, and diluted. Then, 1 mL was inoculated in an agar medium and cultured at 37 °C for 24 h. The number of colonies on each culture surface was counted and analyzed. Each group was repeated three times.

2.6. Characterizations. The crystal structure of ZnS:Mn^{2+} was studied by X-ray diffraction (XRD, D/max-2400, Rigaku, Cu Kα). The morphology of the ZnS:Mn^{2+} powder was characterized by the field emission scanning electron microscopy (FE-SEM JSM-6701 F) at a 10 kV acceleration voltage. The mechanical properties of the elastomers were evaluated by a universal testing machine (SHIMADZU AGS-X-500 N). The ML property was tested by fluorescent spectrometry (Omni-λ300i) and collected by a CCD camera (IVAC-316). The tensile test of the ZnS:Mn^{2+}/PDMS elastomer was carried out by a self-made tensile tester with a tensile strain of 50% and a tensile frequency of 3 Hz, respectively. The friction experiment was operated on a rotating friction testing machine (MS-T3001) using a stainless-steel friction pair with a radius of 0.2 mm. The applied load and the rotational speed are set to be 1 N and 200 rpm, respectively. The compression experiment was operated on a universal testing machine (AGS-X 20k N/1k N SHIMADZU). A load of 300 N was applied on the sample with a loading rate of 60 mm/min. The contact angles of elastomer samples were measured by a contact angle measuring instrument (DSA100). The photos of the

https://doi.org/10.1021/acsapm.1c00917
ACS Appl. Polym. Mater. 2021, 3, 5180−5187

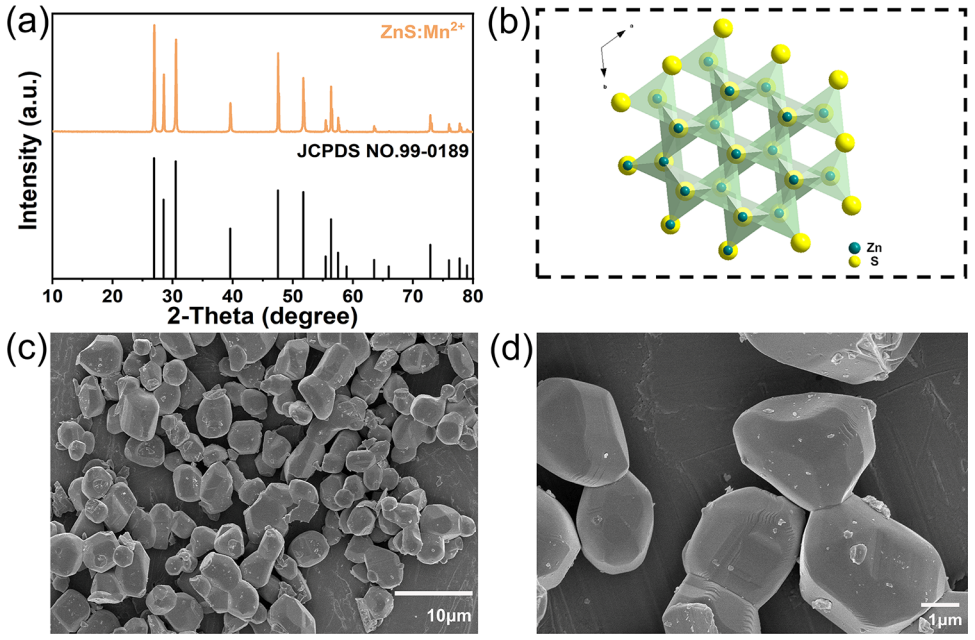

Figure 1. (a) XRD patterns of the as-prepared ZnS:Mn^{2+} and the standard data of the wurtzite ZnS host. (b) Crystal structure of ZnS. SEM images of the as-prepared ZnS:Mn^{2+} powders at (c) 2000× and (d) 10,000× magnifications.

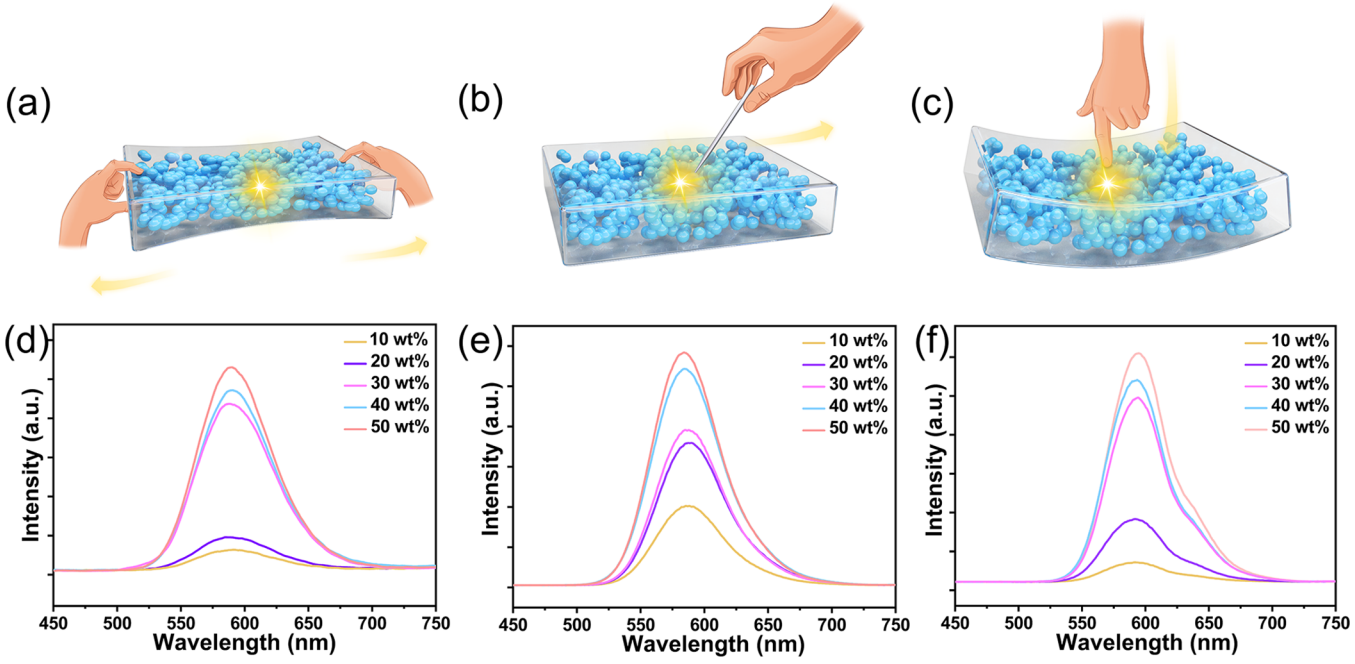

Figure 2. (a–c) ML diagrams of the ZnS:Mn^{2+}/PDMS elastomer under the stimuli of (a) stretching, (b) rubbing, and (c) compressing. (d–f) ML spectra of ZnS:Mn^{2+}/PDMS elastomers with ZnS:Mn^{2+} weight ratios of 10–50% under the (d) tensile (deformation of 50%), (e) friction (load of 1 N), and (f) compression (force of 300 N) stimuli.

occlusion splint model were taken by a digital camera (Canon EOS Rebel T3i). The tribological properties of the ZnS:Mn^{2+}/PDMS elastomers were tested by a CSM reciprocating tribometer under ambient conditions (RH = 30 ± 5%). A zirconium dioxide ball (6 mm diameter) was set as the counterpart. The reciprocating frequency, stroke, and load were 0.5 Hz, 5 mm, and 5 N, respectively. The coefficient of friction was recorded automatically. The abrasive wear of elastomers was derived as below:

$$\Delta V = \frac{m_1 - m_2}{\rho}$$

where ΔV, m_1, m_2, and ρ represent the abrasive wear, the initial and final mass, and the density of the material, respectively. The density is calculated by dividing the quality before the experiment of each sample by its volume.

3. RESULTS AND DISCUSSION

ZnS:1%Mn^{2+} powders were synthesized by the high-temperature solid-state method at 1150 °C for 3 h. Figure 1a shows the XRD patterns of the as-synthesized ZnS:Mn^{2+}. It is observed that the diffraction patterns of the sample well match the standard inorganic crystal structure database (ICSD) card

https://doi.org/10.1021/acsapm.1c00917
ACS Appl. Polym. Mater. 2021, 3, 5180–5187

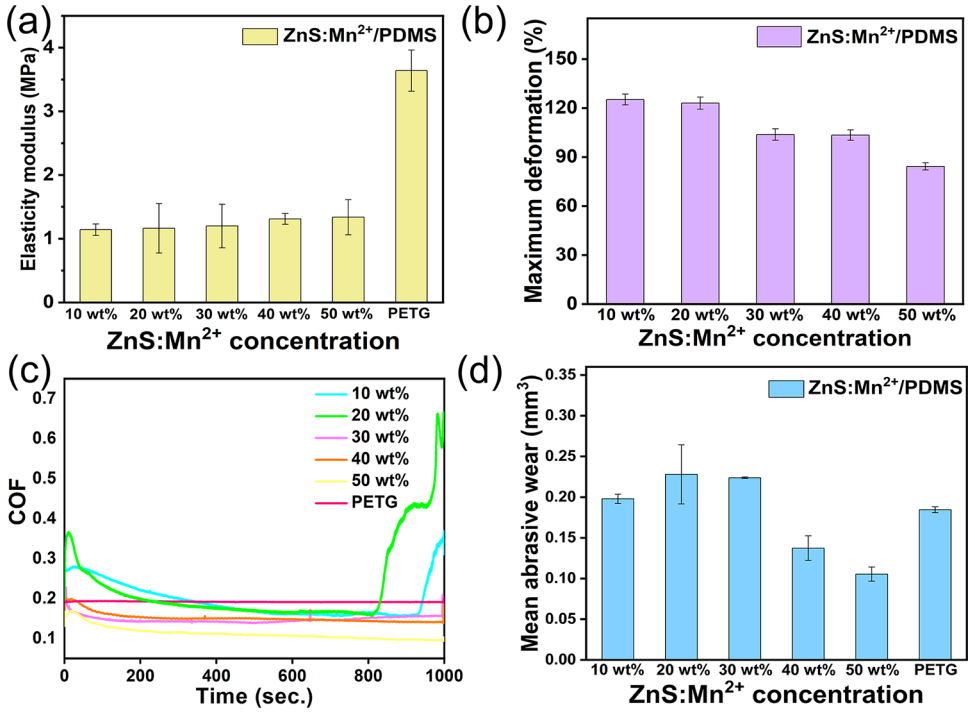

Figure 3. (a) Elasticity modulus of PETG and ZnS:Mn^{2+}/PDMS elastomers with different weight ratios of ZnS:Mn^{2+}. (b) Maximum deformation of ZnS:Mn^{2+}/PDMS elastomers with different weight ratios of ZnS:Mn^{2+}. (c, d) Friction and wear performance of PETG (control group) and ZnS:Mn^{2+}/PDMS elastomers with different weight ratios of ZnS:Mn^{2+}.

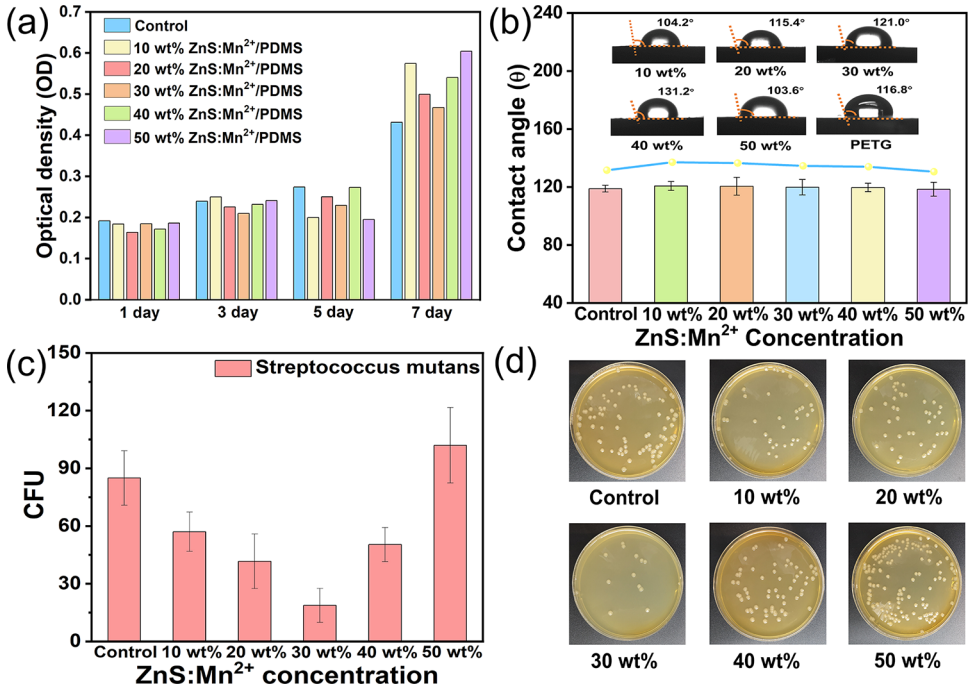

Figure 4. (a) Comparison of optical density of L929 cells after being cultured with ZnS:Mn^{2+}/PDMS elastomers at days 1, 3, 5, and 7. (b) Contact angle of PETG and ZnS:Mn^{2+}/PDMS elastomers with the different weight ratios of ZnS:Mn^{2+}. (c, d) Bacterial agar plate counts of elastomers with different weight ratios of ZnS:Mn^{2+}.

no. 99-0109, suggesting that the single phase of wurtzite ZnS has been obtained.[1] According to the crystal structure in Figure 1b, the wurtzite ZnS is a non-centrally symmetric hexagonal system structure with a space group of *P*63*mc*. Hence, it has high piezoelectricity, which should contribute to the ML performance.[42] From the SEM images of the particles in Figure 1c,d, it is found that the as-prepared ZnS:Mn^{2+} has an irregular polygon morphology with an average size of 3−5 μm. The above results suggest that high-quality ZnS:Mn^{2+} particles with a single phase have been successfully prepared.

To simulate the sophisticated stress situations in human oral cavity during chewing activities,[43] three common types of

https://doi.org/10.1021/acsapm.1c00917
ACS Appl. Polym. Mater. 2021, 3, 5180−5187

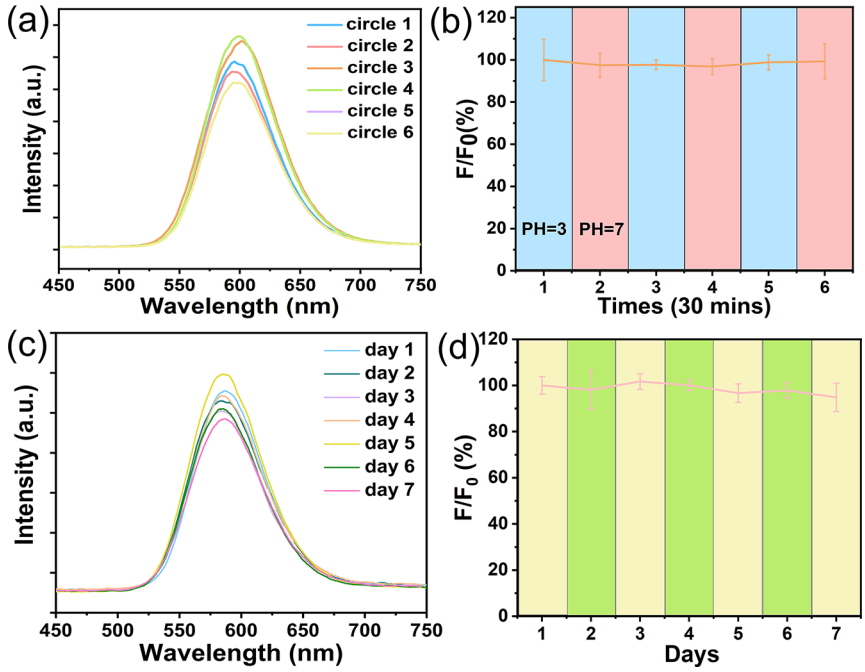

Figure 5. (a, c) ML spectrum and (b, d) physiological stability of the ZnS:Mn^{2+}/PDMS (with a weight ratio of 4:10) occlusal splint under three reversible pH cycles between 7.0 and 3.0 and in artificial saliva at body temperature for different times.

mechanics, i.e., stretching, rubbing, and compressing, are employed to evaluate the ML performance of ZnS:Mn^{2+}/PDMS elastomers, and the corresponding ML processes are illustrated in Figure 2a−c. Figure 2d−f shows the ML spectra of ZnS:Mn^{2+}/PDMS elastomers under the stimuli of stretching, rubbing, and compressing, with the weight ratios of ZnS:Mn^{2+} from 10 to 50%. The measuring conditions for the ones mentioned above are as follows: (1) reaching 50% tensile deformation (Figure 2a,d), (2) scratching via applying 1 N load by a friction machine (Figure 2b,e), and (3) loading 300 N pressure via a universal testing machine (Figure 2c,f). It is found that under whatever measuring conditions, the ML intensity of the ZnS:Mn^{2+}/PDMS elastomers continuously increases with the increase in the content of the ML powders. This shows the potential of the ZnS:Mn^{2+}/PDMS elastomers for occlusal force monitoring.

As a medical device used in human organs for an extended period of treatment, the material for manufacturing occlusal splints is required to have excellent mechanical properties, including abrasion resistance, softness, and comfort. Figure 3 exhibits the results of elastic modulus, deformation, friction, and wear performance of ZnS:Mn^{2+}/PDMS elastomers to investigate their feasibility in occlusal application. All modulus of elasticity for ZnS:Mn^{2+}/PDMS samples at different weight ratios is relatively uniform with values of approximately 1.5 MPa (Figure 3a). Comparing with an elasticity modulus of 3.7 MPa for PETG, a mature commercial occlusal material, the ZnS:Mn^{2+}/PDMS complex has a better softness and comfort property. As shown in Figure 3b, the maximum deformations of ZnS:Mn^{2+}/PDMS samples decrease gradually along the increase in the weight ratio of ZnS:Mn^{2+}, which are all greater than 80%. It means that all candidates can meet the deformation requirement of the material for the occlusal splint. Figure 3c presents the real-time coefficient of friction (COF) for different sample groups. The samples with a weight ratio of ZnS:Mn^{2+} greater than 30% have a lower COF than PETG over the testing period. Furthermore, the curves of the COF for those samples are more stable than the others. Moreover, for the result of average abrasive wear shown in Figure 3d, the mean abrasive wear of the composite materials rises initially with the increment of ZnS:Mn^{2+} doping weight ratio from 10 to 20%. However, the value shows a declining trend when the weight ratio is above 30%. This phenomenon should be aroused by the particle filling effect caused by the high-strength of ZnS:Mn^{2+}. The mechanical test results suggest that the composite elastomers with 40 and 50% weight ratios of ZnS:Mn^{2+} show better properties than the control group.

Biocompatibility, as an important performance index of medical materials,[44,45] has also been systematically studied. Figure 4a shows the result of the proliferation of L929 mouse fibroblasts on the surface of ZnS:Mn^{2+}/PDMS elastomers at days 1, 3, 5, and 7 via the MTT assessment. There is no significant difference between the elastomers and the control group, confirming the biosafety for all samples. Considering the propagation conditions of bacteria, high hydrophobicity could limit the adhesion and cohesion of bacteria, and thus hindering the propagation of bacteria. Figure 4b presents the water contact angles of the as-fabricated ZnS:Mn^{2+}/PDMS elastomers. It can be seen that all of the elastomers exhibit excellent hydrophobicity for antibacterial properties. In addition, *Streptococcus mutans* (MS) were cultivated with different ZnS:Mn^{2+}/PDMS elastomers to evaluate the antibacterial properties, as shown in Figure 4c,d. With the increase in the weight ratios of ZnS:Mn^{2+}, the MS colony counts shrink gradually and reach a minimum at a weight ratio of 30%. It indicates that the composition of ZnS:Mn^{2+} powders in a PDMS elastomer could further improve the antibacterial property, which should be attributed to the Zn^{2+} effect. However, as the weight ratios of ZnS:Mn^{2+} continually increases, the colony counts increase to a higher level than the control group, implying the deterioration of antibacterial properties. This should be caused by the increased surface roughness of the elastomer that is more favorable for bacterial growth.

https://doi.org/10.1021/acsapm.1c00917
ACS Appl. Polym. Mater. 2021, 3, 5180−5187

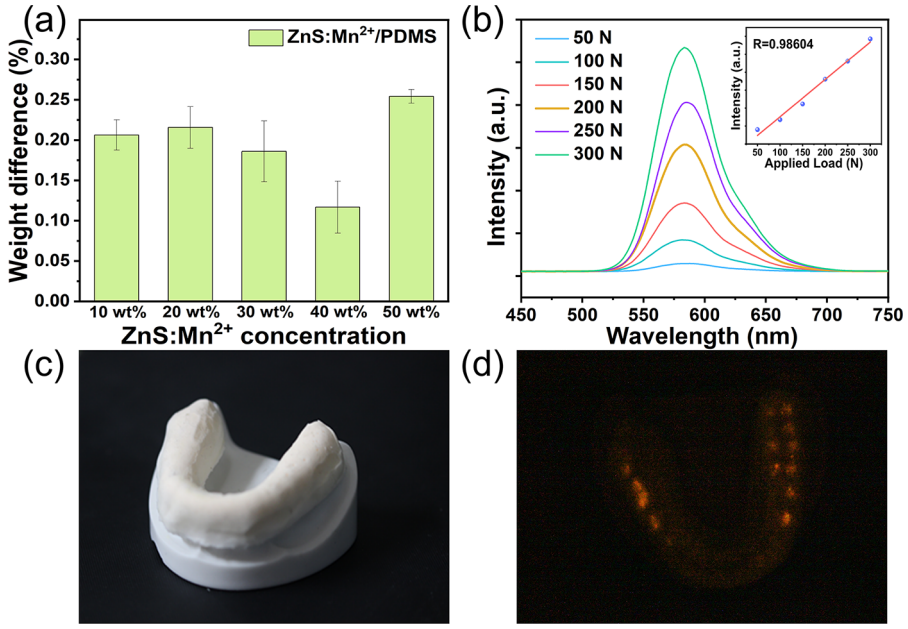

Figure 6. (a) Average solubility of the PETG and ZnS:Mn^{2+}/PDMS elastomer with different weight ratios of ZnS:Mn^{2+} in artificial saliva for 15 days. (b) ML spectra of the ZnS:Mn^{2+}/PDMS elastomer with a weight ratio of 4:10 under a compressing load of 50−300 N. (c) Optical and (d) ML photos of the occlusal splint fabricated from the ZnS:Mn^{2+}/PDMS elastomer.

Based on the above experimental results, the elastomer with a ZnS:Mn^{2+} to PDMS weight ratio of 4:10 was chosen as the most suitable candidate to produce occlusal splint. To ensure the ML stability of the elastomer in an actual clinic treatment, we simulated oral conditions using artificial saliva and confined the temperature at the human body temperature of 37 ± 0.5 °C. Considering that the pH value of natural saliva is relatively neutral and in a range of 5−7, we designed an experimental cycle to soak the elastomers in an extremely acidic environment (pH = 3) for 30 min and shifted to the neutral environment (pH = 7) for another 30 min. As shown in Figure 5a,b, the ML performance of the ZnS:Mn^{2+}/PDMS elastomer has excellent stability under oral conditions. Furthermore, the ML intensity change of the elastomer for long-term usage under oral environment has also been studied (Figure 5c,d), which demonstrates that the ZnS:Mn^{2+}/PDMS elastomer has remarkable stability under oral conditions.

Recent research studies pointed out that the water absorption and dissolution rate play a critical role in the performance of the composite matrix, especially on the cytotoxicity and tissue inflammation.[46] Therefore, the solubility assessment was carried out for each group of the ZnS:Mn^{2+}/PDMS elastomer to further explore the capacity of elastomers for occlusal application. Figure 6a presents the mean weight change by soaking the sample groups in artificial saliva at 37 ± 0.5 °C for 15 days. Overall, the dissolution rate shows a trend of first decreasing and then increasing within an ignorable range of mass, suggesting its excellent dissolution stability for use as an occlusal splint. Figure 6b shows the linear relation between the applied load and the ML intensity of the ZnS:Mn^{2+}/PDMS elastomer with a weight ratio of 4:10, demonstrating the mechanics sensitivity of the candidate elastomer. Therefore, the emitted ML signals under mechanics stimuli could help us to visualize the magnitude of the force during occlusion examination. Herein, a prototype of the soft occlusal splint, using the ZnS:Mn^{2+}/PDMS elastomer with a weight ratio of 4:10, was manufactured as shown in Figure 6c. The corresponding ML photo under compressing is displayed in Figure 6d. It verifies the feasibility of using the ZnS:Mn^{2+}/PDMS elastomer for clinical treatment and force monitoring via the visible ML signals induced by occlusion. It should be noted that after establishing the occlusal equilibration, the occlusal splint could lose its ML performance because of the consumption of the prestored carriers in ZnS:Mn^{2+}.[41] When the occlusal splint requires to be rebalanced, the ML performance can be easily recovered by an irradiation of ultraviolet light for 5 s. Therefore, the developed occlusal splint shows desirable flexibility with no adverse impact on daily wearing.

4. CONCLUSIONS

In summary, a set of ZnS:Mn^{2+}/PDMS elastomers with different mass ratios of ZnS:Mn^{2+} powder were prepared, and the various properties of elastomers were investigated. Comparing with the commercial occlusal splint material, the chosen ZnS:Mn^{2+}/PDMS elastomer with a mass ratio of 40% ML powder shows better elasticity, softness, and wear resistance. Moreover, the excellent biosafety and antibacterial properties of the complex are verified though the biological experiments. The ML of ZnS:Mn^{2+}/PDMS shows a linear relationship to the applied load, providing a visualized strategy for the occlusal inspection. As a result, a prototype of mechanoluminescent splint with desirable mechanical and biological performance as well as the function of visualized occlusal inspection was fabricated, which is promising to be applied in occlusal splint therapy applications.

AUTHOR INFORMATION

Corresponding Authors

Bin Liu − *School/Hospital of Stomatology, Lanzhou University, Lanzhou 730000, China*; Email: liubkq@lzu.edu.cn

Zhaofeng Wang − *State Key Laboratory of Solid Lubrication, Lanzhou Institute of Chemical Physics, Chinese Academy of*

https://doi.org/10.1021/acsapm.1c00917
ACS Appl. Polym. Mater. 2021, 3, 5180−5187

Sciences, Lanzhou, Gansu 730000, China; orcid.org/0000-0003-3641-7011; Phone: +86-931-4968682; Email: zhfwang@licp.cas.cn

Authors

Yue Han − *School/Hospital of Stomatology, Lanzhou University, Lanzhou 730000, China; State Key Laboratory of Solid Lubrication, Lanzhou Institute of Chemical Physics, Chinese Academy of Sciences, Lanzhou, Gansu 730000, China*

Yongqing Bai − *State Key Laboratory of Solid Lubrication, Lanzhou Institute of Chemical Physics, Chinese Academy of Sciences, Lanzhou, Gansu 730000, China;* orcid.org/0000-0002-5710-1756

Jiali Bian − *State Key Laboratory of Solid Lubrication, Lanzhou Institute of Chemical Physics, Chinese Academy of Sciences, Lanzhou, Gansu 730000, China*

Xiuping Guo − *State Key Laboratory of Solid Lubrication, Lanzhou Institute of Chemical Physics, Chinese Academy of Sciences, Lanzhou, Gansu 730000, China*

Complete contact information is available at: https://pubs.acs.org/10.1021/acsapm.1c00917

Notes

The authors declare no competing financial interest.

■ ACKNOWLEDGMENTS

This work was supported by the National Natural Science Foundation of China (81970976) and the Natural Science Foundation for Distinguished Young Scholars of Gansu Province (20JR5RA572).

■ REFERENCES

(1) Gil-Martínez, A.; Paris-Alemany, A.; López-de-Uralde-Villanueva, I.; la Touche, R. Management of Pain in Patients with Temporomandibular Disorder (TMD): Challenges and Solutions. *J. Pain Res.* **2018**, *Volume 11*, 571−587.

(2) Ferreira, F. M.; Simamoto-Júnior, P. C.; Soares, C. J.; de Amaral Monteiro Ramos, A. M.; Fernandes-Neto, A. J. Effect of Occlusal Splints on the Stress Distribution on the Temporomandibular Joint Disc. *Brazilian Dent. J.* **2017**, *28*, 324−329.

(3) Ingawalé, S.; Goswami, T. Temporomandibular Joint: Disorders, Treatments, and Biomechanics. *Annals of Biomedical Enginee.* **2009**, *37*, 976−996.

(4) McNeill, C. Management of Temporomandibular Disorders: Concepts and Controversies. *J. Prosthetic Dent.* **1997**, *77*, 510−522.

(5) Magnusson, T.; Egermark, I.; Carlsson, G. E. A Longitudinal Epidemiologic Study of Signs and Symptoms of Temporomandibular Disorders from 15 to 35 Years of Age. *J. Orofacial Pain* **2000**, *14*, 310−319.

(6) Dzingutė, A.; Pileičikienė, G.; Baltrušaitytė, A.; Skirbutis, G. Evaluation of the Relationship between the Occlusion Parameters and Symptoms of the Temporomandibular Joint Disorder. *Acta medica Lituanica* **2017**, *24*, 167−175.

(7) Turkistani, K. A.; Alkayyal, M. A.; Abbassy, M. A.; Al-Dharrab, A. A.; Zahran, M. H.; Melis, M.; Zawawi, K. H. Comparison of Occlusal Bite Force Distribution in Subjects with Different Occlusal Characteristics. *Cranio - Journal of Craniomandibular Practice* **2020**, 1−8.

(8) Ohnuki, T.; Fukuda, M.; Nakata, A.; Nagai, H.; Takahashi, T.; Sasano, T.; Miyamoto, Y. Evaluation of the Position, Mobility, and Morphology of the Disc by MRI before and after Four Different Treatments for Temporomandibular Joint Disorders. *Dentomaxillofacial Radiology* **2006**, *35*, 103−109.

(9) Nagori, S. A.; Jose, A.; Roy Chowdhury, S. K.; Roychoudhury, A. Is Splint Therapy Required after Arthrocentesis to Improve Outcome in the Management of Temporomandibular Joint Disorders? A Systematic Review and Meta-Analysis. *Oral Surgery, Oral Medicine, Oral Pathology and Oral Radiology.* **2019**, *127*, 97−105.

(10) Al-Moraissi, E. A.; Farea, R.; Qasem, K. A.; Al-Wadeai, M. S.; Al-Sabahi, M. E.; Al-Iryani, G. M. Effectiveness of Occlusal Splint Therapy in the Management of Temporomandibular Disorders: Network Meta-Analysis of Randomized Controlled Trials. *Inter. J. Oral Maxillofacial Surg.* **2020**, *49*, 1042−1056.

(11) dos Santos Marsico, V.; Lehmann, R. B.; de Assis Claro, C. A.; Amaral, M.; Vitti, R. P.; Neves, A. C. C.; da Silva Concilio, L. R. Three-Dimensional Finite Element Analysis of Occlusal Splint and Implant Connection on Stress Distribution in Implant−Supported Fixed Dental Prosthesis and Peri-Implantal Bone. *Mater. Sci. Eng., C* **2017**, *80*, 141−148.

(12) Alqutaibi, A. Y.; Aboalrejal, A. N. Types of Occlusal Splint in Management of Temporomandibular Disorders (TMD). *J. Arthritis* **2015**, *04*, 1000176.

(13) Seifeldin, S. A.; Elhayes, K. A. Soft versus Hard Occlusal Splint Therapy in the Management of Temporomandibular Disorders (TMDs). *Saudi Dent. J.* **2015**, *27*, 208−214.

(14) Amin, A.; Meshramkar, R.; Lekha, K. Comparative Evaluation of Clinical Performance of Different Kind of Occlusal Splint in Management of Myofascial Pain. *J. Indian Prosthodont. Soc.* **2016**, *16*, 176−181.

(15) Gholampour, S.; Gholampour, H.; Khanmohammadi, H. Finite Element Analysis of Occlusal Splint Therapy in Patients with Bruxism. *BMC Oral Health* **2019**, *19*, 205.

(16) Barão, V. A. R.; Gallo, A. K. G.; Zuim, P. R. J.; Garcia, A. R.; Assunção, W. G. Effect of Occlusal Splint Treatment on the Temperature of Different Muscles in Patients with TMD. *J. Prosthodontic Res.* **2011**, *55*, 19−23.

(17) Reyes-Sevilla, M.; Kuijs, R. H.; Werner, A.; Kleverlaan, C. J.; Lobbezoo, F. Comparison of Wear between Occlusal Splint Materials and Resin Composite Materials. *J. Oral Rehab.* **2018**, *45*, 539−544.

(18) Benli, M.; Eker Gümüş, B.; Kahraman, Y.; Gökçen-Rohlig, B.; Evlioğlu, G.; Huck, O.; Özcan, M. Surface Roughness and Wear Behavior of Occlusal Splint Materials Made of Contemporary and High-Performance Polymers. *Odontology* **2020**, *108*, 240−250.

(19) Domanic, K. Y.; Aslan, Y. U.; Ozkan, Y. Two-Body Wear of Occlusal Splint Materials against Different Antagonists. *BMC Oral Health* **2020**, *20*, 1−7.

(20) Gould, T. E.; Piland, S. G.; Shin, J.; Hoyle, C. E.; Nazarenko, S. Characterization of Mouthguard Materials: Physical and Mechanical Properties of Commercialized Products. *Dent. Mater.* **2009**, *25*, 771−780.

(21) Afrashtehfar, K. I.; Qadeer, S. Computerized Occlusal Analysis as an Alternative Occlusal Indicator. *Cranio* **2016**, *34*, 52−57.

(22) Sharma, A.; Rahul, G. R.; Poduval, S. T.; Shetty, K.; Gupta, B.; Rajora, V. History of Materials Used for Recording Static and Dynamic Occlusal Contact Marks: A Literature Review. *J. Clin. Exp. Dent.* **2012**, *5*, e48−e53.

(23) Mitchem, J. A.; Katona, T.; Moser, E. A. S. R.; Moser, E. A. S. Does the Presence of an Occlusal Indicator Product Affect the Contact Forces between Full Dentitions? *J. Oral Rehabil.* **2017**, *44*, 791−799.

(24) Forrester, S. E.; Presswood, R. G.; Toy, A. C.; Pain, M. T. G. Occlusal Measurement Method Can Affect SEMG Activity during Occlusion. *J. Oral Rehab.* **2011**, *38*, 655−660.

(25) Carey, J. P.; Craig, M.; Kerstein, R. B.; Radke, J. Determining a Relationship Between Applied Occlusal Load and Articulating Paper Mark Area. *Open Dent. J.* **2007**, *1*, 1−7.

(26) Kerstein, R. B. Articulating Paper Mark Misconceptions and Computerized Occlusal Analysis Technology. *Dent. implantology update* **2008**, *19*, 41−46.

(27) Kerstein, R. B.; Radke, J. Clinician Accuracy When Subjectively Interpreting Articulating Paper Markings. *Cranio* **2014**, *32*, 13−23.

(28) Tian, B.; Wang, Z.; Smith, A. T.; Bai, Y.; Li, J.; Zhang, N.; Xue, Z.; Sun, L. Stress-Induced Color Manipulation of Mechanolumines-

cent Elastomer for Visualized Mechanics Sensing. *Nano Energy* **2021**, *83*, 105860.
(29) Zhuang, Y.; Xie, R.-J. Mechanoluminescence Rebrightening the Prospects of Stress Sensing: A Review. *Adv. Mater.* **2021**, 2005925.
(30) Wang, C.; Yu, Y.; Yuan, Y.; Ren, C.; Liao, Q.; Wang, J.; Chai, Z.; Li, Q.; Li, Z. Heartbeat-Sensing Mechanoluminescent Device Based on a Quantitative Relationship between Pressure and Emissive Intensity. *Matter* **2020**, *2*, 181−193.
(31) Zhang, J.-C.; Pan, C.; Zhu, Y.-F.; Zhao, L.-Z.; He, H.-W.; Liu, X.; Qiu, J. Achieving Thermo-Mechano-Opto-Responsive Bitemporal Colorful Luminescence via Multiplexing of Dual Lanthanides in Piezoelectric Particles and Its Multidimensional Anticounterfeiting. *Adv. Mater.* **2018**, *30*, 1804644.
(32) Jeong, S. M.; Song, S.; Kim, H. Simultaneous Dual-Channel Blue/Green Emission from Electro-Mechanically Powered Elastomeric Zinc Sulphide Composite. *Nano Energy* **2016**, *21*, 154−161.
(33) Bian, J.; Han, Y.; Wang, F.; Liu, B.; Li, H.; Wang, Z. Enhanced Mechanoluminescence of ZnS:Mn2+ in Flexible Polyurethane via Interfacial Interactions. *Mater. Res. Bull.* **2021**, *140*, 111295.
(34) Jiang, Y.; Wang, F.; Zhou, H.; Fan, Z.; Wu, C.; Zhang, J.; Liu, B.; Wang, Z. Optimization of Strontium Aluminate-Based Mechanoluminescence Materials for Occlusal Examination of Artificial Tooth. *Mater. Sci. Eng., C* **2018**, *92*, 374−380.
(35) Ji, Z.; Jiang, D.; Zhang, X.; Guo, Y.; Wang, X. Facile Photo and Thermal Two-Stage Curing for High-Performance 3D Printing of Poly(Dimethylsiloxane). *Macromol. Rapid Commun.* **2020**, *41*, 20000064.
(36) Döhler, D.; Kang, J.; Cooper, C. B.; Tok, J. B.-H.; Rupp, H.; Binder, W. H.; Bao, Z. Tuning the Self-Healing Response of Poly(Dimethylsiloxane)-Based Elastomers. *ACS Appl. Polym. Mater.* **2020**, *2*, 4127−4139.
(37) Toole, B. P. Hyaluronan in Morphogenesis. *Sem. Cell Dev. Biol.* **2001**, *12*, 79−87.
(38) Toole, B. P. Hyaluronan: From Extracellular Glue to Pericellular Cue. *Nat. Rev. Cancer* **2004**, *4*, 528−539.
(39) Mohania, V.; Deshpande, T. D.; Singh, Y. R. G.; Patil, S.; Mangal, R.; Sharma, A. Fabrication and Characterization of Porous Poly(Dimethylsiloxane) (PDMS) Adhesives. *ACS Appl. Polym. Mater.* **2021**, *3*, 130−140.
(40) Wang, X.; Zhang, H.; Yu, R.; Dong, L.; Peng, D.; Zhang, A.; Zhang, Y.; Liu, H.; Pan, C.; Wang, Z. L. Dynamic Pressure Mapping of Personalized Handwriting by a Flexible Sensor Matrix Based on the Mechanoluminescence Process. *Adv. Mater.* **2015**, *27*, 2324−2331.
(41) Zhou, H.; Du, Y.; Wu, C.; Jiang, Y.; Wang, F.; Zhang, J.; Wang, Z. Understanding the Mechanoluminescent Mechanisms of Manganese Doped Zinc Sulfide Based on Load Effects. *J. Lumin.* **2018**, *203*, 683−688.
(42) Chandra, B. P.; Chandra, V. K.; Jha, P. Elastico-Mechanoluminescence and Crystal-Structure Relationships in Persistent Luminescent Materials and II-VI Semiconductor Phosphors. *Phys. B* **2015**, *463*, 62−67.
(43) Marek, M. Interactions between Dental Amalgams and the Oral Environment. *Adv. dent. research.* **1992**, *6*, 100−109.
(44) Cui, B.; Zhang, R.; Sun, F.; Ding, Q.; Lin, Y.; Zhang, L.; Nan, C. Mechanical and Biocompatible Properties of Polymer-Infiltrated-Ceramic-Network Materials for Dental Restoration. *J. Adv. Ceram.* **2020**, *9*, 123−128.
(45) Feng, C.; Zhang, K.; He, R.; Ding, G.; Xia, M.; Jin, X.; Xie, C. Additive Manufacturing of Hydroxyapatite Bioceramic Scaffolds: Dispersion, Digital Light Processing, Sintering, Mechanical Properties, and Biocompatibility. *J. Adv. Ceram.* **2020**, *9*, 360−373.
(46) Liang, X.; Liu, F.; He, J. Synthesis of None Bisphenol A Structure Dimethacrylate Monomer and Characterization for Dental Composite Applications. *Dent. Mater.* **2014**, *30*, 917−925.

https://doi.org/10.1021/acsapm.1c00917
ACS Appl. Polym. Mater. 2021, 3, 5180−5187